Invited Paper

Tunable optical properties of photonic crystals and semiconductor microdisks using liquid crystals

Karoline A. Piegdon[(1)], Heinrich Matthias[(2)], Cedrik Meier[(1)], and Heinz-S. Kitzerow[(2)(*)]

[(1)]Experimental Physics and CeNIDE, University of Duisburg-Essen,
Lotharstr. 1, 47057 Duisburg, Germany
[(2)]Faculty of Science, Physical Chemistry, University of Paderborn,
Warburger Str. 100, 33098 Paderborn, Germany

ABSTRACT

The combination of semiconductors and liquid crystals is extremely useful in order to fabricate integrated optical devices with tunable properties. The difference between the dielectric constants of the semiconductor and the liquid crystal ('dielectric contrast') is sufficiently high to obtain photonic band gap structures or resonant microcavities with high quality factor. At the same time, the characteristic frequencies can be controlled by temperature changes or external fields due to the thermo-, electro- or magneto-optic sensitivity of the liquid crystal. Here, previous investigations on microcavities embedded in silicon-based photonic crystals are reviewed and new results on integrated GaAs microdisks containing a light emitting layer of InAs quantum dots are presented. The latter show resonant modes with a typical width below 0.4 nm in the near infrared spectral range around 1.24 µm, which indicates a quality factor of 3500 and larger. By embedding a microdisk in a well-aligned liquid crystal and subsequent heating to the isotropic phase, a spectral shift of about 7 nm was observed. The results indicate a possible way of developing tunable light sources.

Keywords: Photonic crystals, microdisks, liquid crystals, tunable resonance frequency.

1. INTRODUCTION

Using light rather than electric currents in information technology is one of the big challenges of the 21st century. Thus, exploring photonic effects and developing novel photonic and integrated optical devices is a major issue of topical research and development. The devices to be applied for this purpose need geometrical fine structures not larger than the wavelength of the respective radiation and fabrication accuracies that are much smaller than the wavelength. Methods of tuning the photonic properties are necessary in order to both compensate fabrication tolerances and to achieve active switching.

Among the materials to be used for addressable photonic devices, liquid crystals are promising candidates since their effective refractive indices and susceptibilities are very sensitive to temperature and external fields. Calamitic liquid crystals (Fig. 1) are ordered liquids that consist of rod like molecules, which align preferentially parallel to each other thereby leading to uniaxial birefringence. The preferred orientation of the molecules (described by a pseudo-vector, the director **n**) corresponds to the local optical axis. In the non-chiral nematic phase, which is characterized by uniform alignment, the degree of orientational order (described by the scalar order parameter S) is related to the difference $\Delta n = n_e - n_o$ between the extraordinary refractive index n_e and the ordinary refractive index n_o. The orientation of the optical axis and the birefringence Δn can be controlled by external fields and by adjusting the temperature, respectively. Consequently, liquid crystals have been applied to make micro and nanostructures tunable.


[(*)] e-mail: Heinz.Kitzerow@upb.de; internet: http://www.ceopp.de/
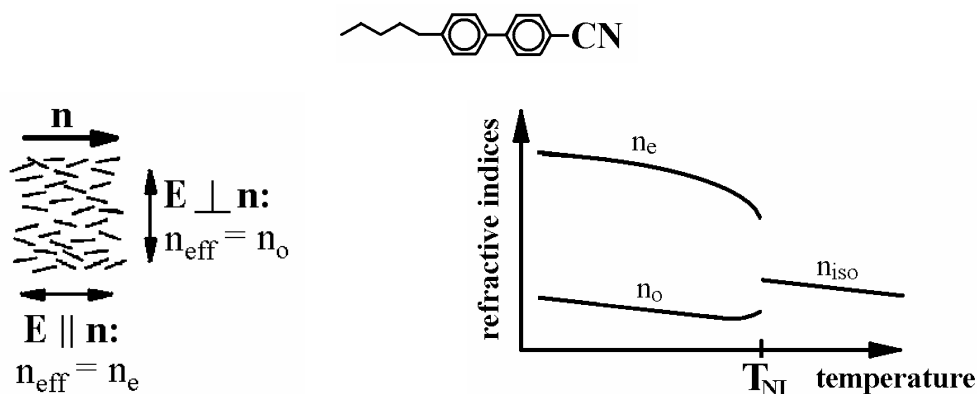
Figure 1. Top: Molecular structure of the liquid crystal 5CB. **Lower left:** Arrangement of rod-like molecules in the nematic phase and definition of the director **n**. For polarized light, the effective refractive index corresponds to the extraordinary refractive index n_e when the electric field vector **E** of the light is parallel to **n** and to the ordinary refractive index n_o when **E** is perpendicular to **n**, respectively. **Lower right:** Schematic temperature dependence of the refractive indices.

The use of liquid crystals has been successfully applied to photonic crystals [1-3]. It was first proposed [4] and experimentally demonstrated [5] for model systems composed of self-organized colloidal particles. After successful proofs of principle, the use of liquid crystals was soon extended to semiconductor structures which are much more robust and more suitable for practical applications. Both photonic crystals made of macroporous silicon [6-10] and optoelectronic III-V semiconductors [11,12] were successfully infiltrated with liquid crystals in order to achieve tunable properties. The ordinary refractive index n_o and the extraordinary refractive index n_e of the liquid crystal are typically $n_o \approx 1.5$ (± 0.1) and $n_e \approx 1.7$ (± 0.1). Thus, the dielectric contrast to the semiconductor is sufficiently large to open photonic stop bands. Typically, the edges of the stop bands or the resonance frequency of a defect mode can be spectrally shifted by about 1 % due to changes of the temperature or application of external fields. Reithmaier et al. succeeded to fabricate tunable photonic crystals fabricated in III-V semiconductor slab waveguides where a wavelength jump of about 4 nm within a few Kelvin and a total shift of 9 nm on heating from 20 to 70°C could be observed. Maune et al. [12] demonstrated an electrically tuned nematic liquid crystal-infiltrated photonic crystal laser based on an InGaAsP quantum well structure, where a blue shift of the emission wavelength of 1.2 nm could be achieved by applying a voltage of 20 V.

The example of a photonic crystal made of macroporous silicon filled with a liquid crystal [8] is shown in the Fig. 2. In a two dimensional square lattice of macropores with a lattice constant of a = 2 μm, the pore diameter D was periodically modulated $D_{min} = 0.92$ μm and $D_{max} = 1.55$ μm with a spatial periodicity of 2.58 μm. A planar microcavity was generated inside this 3D photonic crystal by varying the pore diameter periodically along the pore axis, allowing it to remain constant within a defect layer and then continuing the periodic modulation. For infrared radiation propagating along the pore axes, experiments showed a transmission peak at λ = 7.184 μm in the center of the second stop band, which can be attributed to a localized defect mode. After filling the structure with the liquid crystal 4-cyano-4'-pentyl-biphenyl (5CB, Merck) a temperature-induced shift by Δλ = 20 nm from λ = 7.375 μm to λ = 7.395 μm was observed when the liquid crystal was heated from 24°C (nematic phase) to 40°C (isotropic liquid phase). The shift toward larger wavelengths indicates an increase of the effective refractive index n_{eff} of the liquid crystal with increasing temperature and can be attributed to the transition from an initially parallel aligned nematic phase ($n_{LC,eff} = n_o$) to the isotropic state ($n_{LC,eff} = n_{iso}$). Continuous variation of the temperature revealed a distinct step by 20 nm in a very narrow temperature region that corresponds to the phase transition from the nematic to the isotropic phase. This interesting effect and the subsequent studies about the details of the liquid crystal director fields in modulated pores have been reviewed, recently [3].
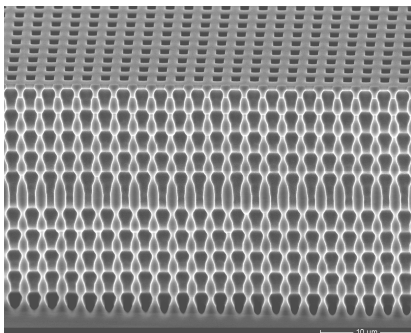
Figure 2. Scanning electron microscopy (SEM) image of a resonant microcavity in a photonic crystal made of silicon. The two dimensional square lattice of modulated pores contains a planar microresonator (pore diameter D = 0.920 - 1.546 μm, lattice constant in the plane a = 2 μm, lattice constant along the pore axes c = 2.577 μm, resonator gap l = 2.65 μm). For details, see Ref. [8].
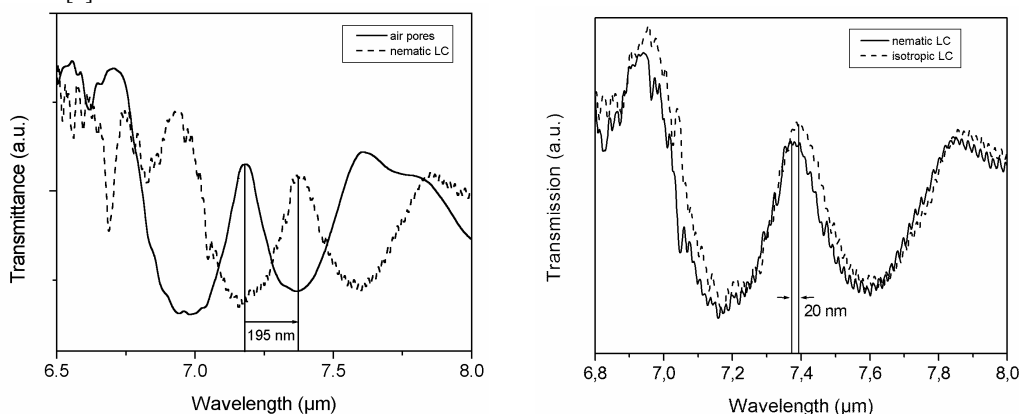
Figure 3. IR transmission spectra of the photonic crystal structure shown in Figure 2. **Left:** Stop band and resonance peak observed along the Γ-A direction for pores filled with air (solid line) and filled with 5CB (dashed line), respectively. **Right:** Spectral position of the resonance peak of the filled structure at 24 °C (nematic phase, solid line) and 40 °C (isotropic phase, dashed line), respectively. For details, see Ref. [8].

2. WHISPERING GALLERY MODES OF MICRODISKS AND EXPECTED INFLUENCE OF THE DIELECTRIC ENVIRONMENT

Semiconductor microdisks (Fig. 4) are microfabricated flat cylindrical objects that are known as optical microresonators with the potential of large quality factors. They can be used for enhancement of the stimulated emission and are very promising for laser applications. The resonant modes correspond to two-dimensional standing waves with radial symmetry, usually referred to as whispering gallery modes. They can be classified by two quantum numbers, a radial quantum number N and an azimuthal quantum number M, where (N-1) indicates the number of nodes along the radial direction and M corresponds to the number of nodes along the periphery [13]. For example, the electric field distribution for light polarized in the plane of the disk is given in cylindrical coordinates by $E_y(r,\varphi) = J_M(\rho) \cdot \exp(i \cdot M \cdot \varphi)$, where $J_M(\rho)$ are the Bessel functions of the first kind and $\rho = n \cdot \omega \cdot r / c$ (with n being the effective refractive index) is a reduced radial coordinate. For the ideal case of an infinite potential barrier at the disk edge and assuming a fixed radial quantum number N = 1, the frequency of a mode with quantum number M is, for example, given by $\omega = n \cdot c \cdot r / M$. The eigenmodes are mostly localized inside the high-index semiconductor material. However, a small fraction of the electromagnetic field decays exponentially in the surrounding medium, i. e., either air or the liquid crystal. Due to the strong confinement, the evanescent field strength is larger in the z-direction than in the (x,y)-plane. The evanescent decay length depends on the mode wavelength, disk thickness, and index contrast between the surrounding material and the semiconductor. For the wavelengths and materials studied here, it is in the range of 100-300nm.
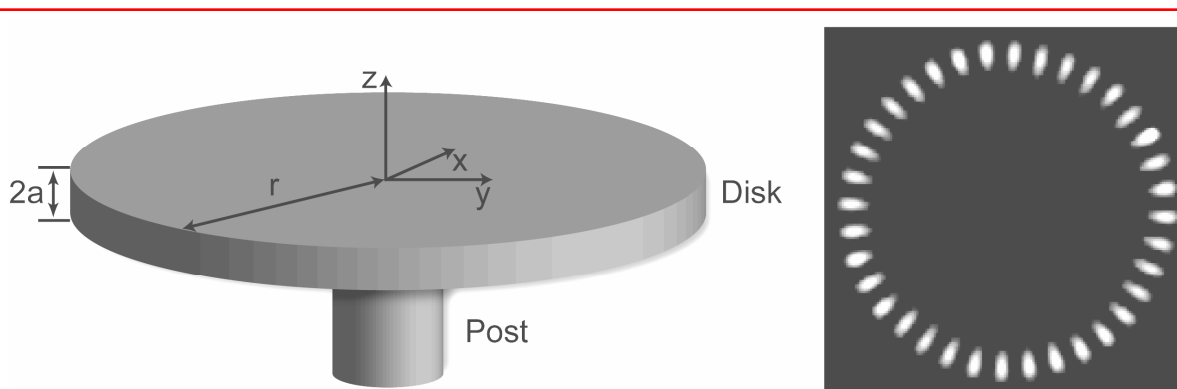
Figure 4. Left: Design and important parameters of a microdisk. **Right:** Simulation of the electric field distribution of a whispering gallery mode with low radial quantum number in a microdisk made of GaAs.

3. FABRICATION OF MICRODISKS EMBEDDED IN A LIQUID CRYSTAL

All samples were fabricated from an epitaxial structure, which was grown by all solid source molecular beam epitaxy (MBE) on a 600 µm thick semi-insulating GaAs (100) substrate. The layer structure starts with 300 nm Si doped GaAs. This conducting layer can be electrically contacted and used as a back contact. On top, the 500 nm $Al_{0.33}Ga_{0.67}As$ sacrificial layer was grown. Above the sacrificial layer, the active membrane follows, which consists of 240 nm GaAs with an embedded layer of (In,Ga)As self-assembled quantum dots (QDs) in the center of the GaAs. To obtain a photoluminescence signal with sufficient intensity at room temperature, the QDs were grown with a comparably high In-content, leading to a photoluminescence emission in the range of 1100 nm – 1250 nm.

Photolithography was used to define circular mesas with diameters ranging from 5 to 7 µm. The lithographic steps are shown in Fig. 5. The substrate was covered by a photoresist for the first etching step. Here, an HBr based solution is used to etch the disk- and the sacrificial layer. The used etching solution consists of 3.6 g $K_2Cr_2O_7$ dissolved in 25 ml de-ionized water, 25 ml $C_2H_4O_2$ (99%) and 25 ml HBr (47%). Diluted with de-ionized water in the ratio 1:4, the typical etch rate was 1.8 µm/min. Due to the isotropic etching of the diluted solution, vertical microdisk edges were formed in this step in the GaAs membrane region. A secondary electron micrograph (SEM) of the resulting GaAs mesa can be seen in figure 6 (to the left).
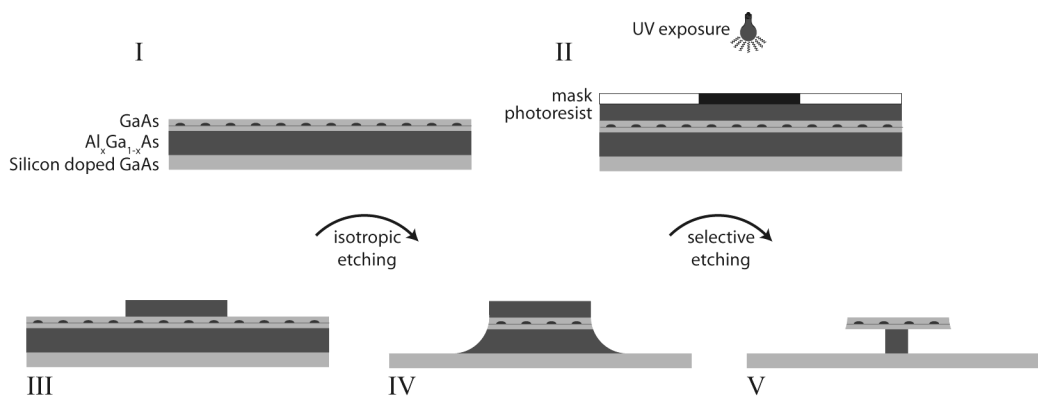
Figure 5. Fabrication steps of the microdisks. I) Initial wafer, II) photolithography, III) protection layer after development, IV) isotropic etching, V) selective etching.

After this step, the pedestal was formed by selective etching of the $Al_{0.33}Ga_{0.67}As$ layer. As a result of the low Al content, an etching solution based on I, KI and H_2SO_4 was used. In Ref. [14], Lau *et al.* found a selectivity of up to 300 in etching $Al_{0.33}Ga_{0.67}As$ in preference over GaAs. To obtain this high selectivity, 13.9 g I_2 and 8.1 g KI were dissolved in de-ionized water and mixed 1:1 with H_2SO_4, where the pH-value was set to 0.9 in an aqueous solution. After cooling down to 4°C, the etch rate of this solution was typically 800 nm/min, strongly dependent on the etch age. The right part of Fig. 6 shows a scanning electron micrograph of the underetched microdisk.

Finally, the microdisks were embedded in the nematic liquid crystal 4-cyano-4'-pentylbiphenyl (5CB), which undergoes a nematic-isotropic phase transition at T_C=34°C and has a melting point of T_M=22,5°C. To promote planar alignment at the semiconductor surface, the samples were treated with either diluted MAP (N-Methyl-3-aminopropyltrimethoxysilan) or with PVA [poly(vinyl alcohol)] and then rinsed in de-ionized water. Finally, the devices were capped with a thin glass slide, so that a layer of 5 μm LC remained between glass and semiconductor.
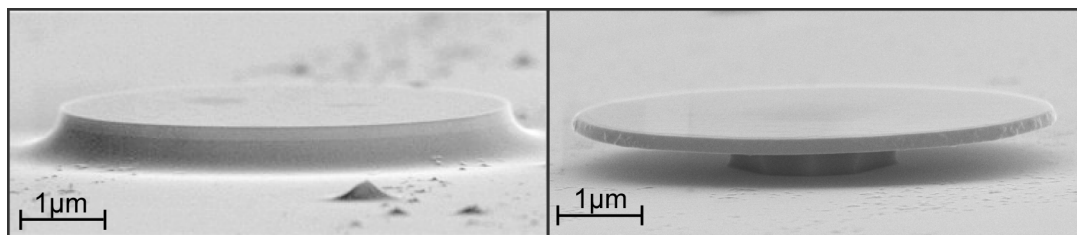

Figure 6. SEM images of the fabricated microdisks.

4. EXPERIMENTAL RESULTS ON MICRODISKS EMBEDDED IN A LIQUID CRYSTAL

The samples were excited using a continuous wave (cw) Ti:sapphire laser operating at 780 nm. The spot size was approximately d=1.7μm. The excitation power density was about 40kW/cm^2 . The photoluminescence light from the sample was dispersed in a Czerny-Turner monochromator. As a detector, a liquid nitrogen cooled (In,Ga)As photodiode array was used. Using this setup, a spectral resolution of 0.3 nm was achieved. The sample was mounted on a copper sample holder with an electric heater. Using PID-control, the temperature could be set with an accuracy of 0.1 K.

In order to study the effects of liquid crystal infiltration it is necessary to investigate the initial photoluminescence spectrum of a microdisk in vacuum or surrounded by air (Fig. 7, to the left). This spectrum shows very narrow peaks on a background of three broad bands at about 1250 nm, 1170nm and 1100nm. The background corresponds to the luminescence of the quantum dots while the narrow peaks indicate the resonant modes of the microresonator. The luminescence of the quantum dots can be roughly described by the model of a two-dimensional symmetric oscillator, which exhibits the energies $E_{n,m} = \hbar \cdot \omega_0 \cdot (n + \frac{1}{2}) + \hbar \cdot \omega_0 \cdot (m + \frac{1}{2}) = \hbar \cdot \omega_0 \cdot (n + m + 1)$, with n = 0, 1, 2, …and m = 0, 1, 2, … being the quantum numbers. The eigenfunctions can also be classified by a quantum number l := n + m, which corresponds to the respective angular momentum. In analogy to atoms, the eigenstates are called "s" (l = 0), "p" (l = 0), "d" (l = 1), and so on. In this notation the three broad bands can be attributed to the transitions s → s' (≈1250 nm), p → p' (≈1170 nm), and d → d' (≈1100 nm), where s, p and d designate the states of an electron in the conduction band and s', p' and d' are the corresponding states of a hole in the valence band of the semiconductor. The peaks that correspond to the microresonator modes have a width that is limited by the spectral resolution of the microphotoluminescence setup. This very narrow width ($< \approx 0.3$ nm) indicates a quality factor Q of the micro disk resonator larger than 4000.

The right part of figure 7 shows the photoluminescence spectrum of a microdisk embedded in the liquid crystal 5CB. Due to the scattering of the excitation laser light in the liquid crystal, the power density on the microdisk is significantly reduced in comparison to the sample without LC. This is the reason for the lower ratio between the photonic mode and the quantum dot emission in the LC immersed sample. However, the larger peaks of resonator modes, on which this study is focused, can still be detected very clearly. In addition, the spectral width is still extremely small, indicating that a very high quality factor of Q ≈ 3500 and larger, is still be preserved if the microdisk is embedded in a liquid crystal.
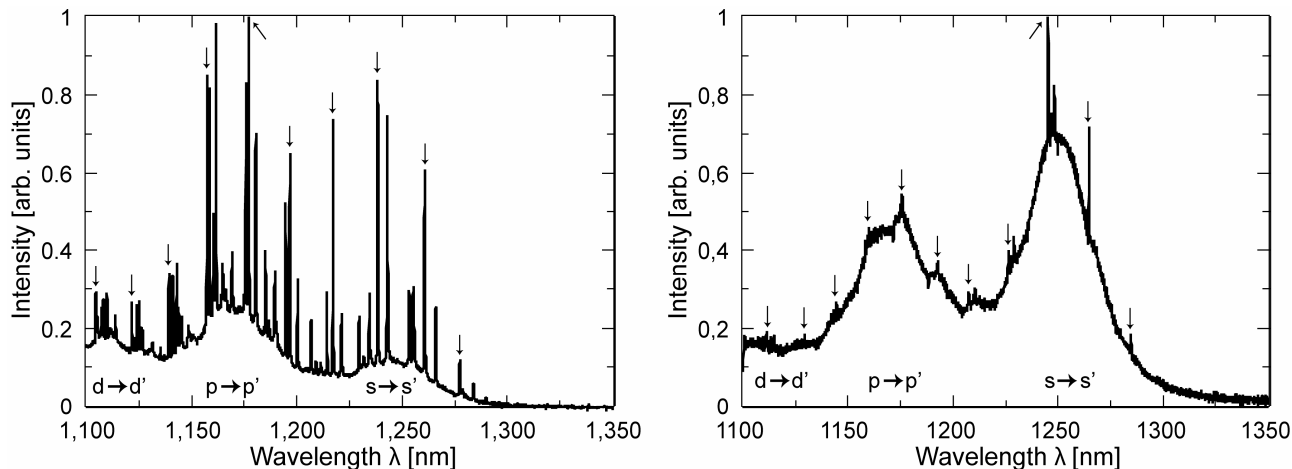
Figure 7. IR spectra of a microdisk with r = 3.268 µm. **Left:** Spectrum of the microdisk surrounded by air. **Right:** Spectrum of the same microdisk embedded in the liquid crystal 5CB.

4.1 Thermal tuning

The microdisk with r = 3 µm embedded in the liquid crystal 5CB shows a remarkable dependence of the resonance wavelengths on temperature. Below the clearing temperature T_{NI}, the peak wavelengths are shifted towards smaller values with increasing temperature (Fig. 8). However, above the clearing point, the peak wavelengths λ are shifted to wards larger values with increasing temperature T. For comparison, Fig. 8 shows the temperature dependence of resonance wavelength in a sample without liquid crystal. In this case, the slope dλ/dT is positive throughout and approximately equal to the slope of the sample with liquid crystal above the clearing temperature. This slope can be attributed to the thermal expansion of the semiconductor, whereas the negative temperature coefficient below T_{NI} is due to anisotropy and the resulting changes of the ordinary and extraordinary refractive indices.
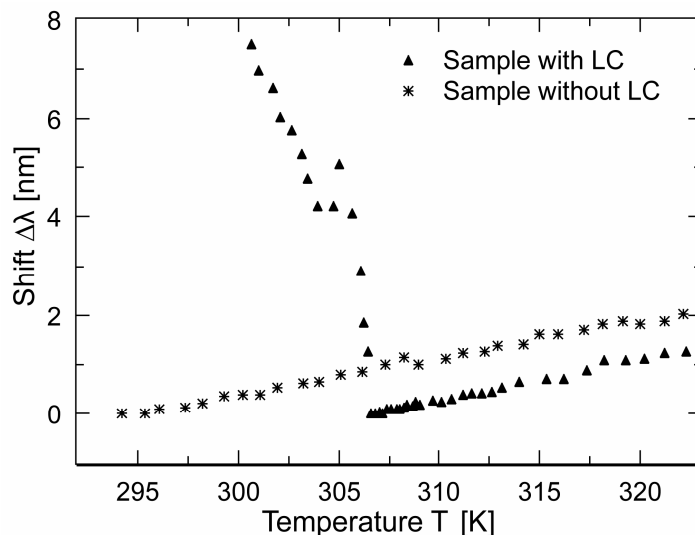
Figure 8. Shift of the resonance wavelengths as a function of temperature for a sample (▲) with and (■) without the liquid crystal 5CB, respectively.

4.2 Electric field-induced tuning

In order to apply electric fields, the samples were placed between two glass plates coated with transparent electrodes made of indium tin oxide (ITO). The distance of the electrodes was approximately 1 mm (Fig. 9). Alternating voltages with a frequency of 50 Hz were applied. With increasing rms-value of the voltage, the resonance wavelengths are shifted towards lower values (Fig. 10). By applying up to 30 V, the peaks can be shifted by several nm, a range similar to the temperature-induced shifts. The corresponding field strengths of $E \leq 300$ V / cm are surprisingly low. Using typical values of $K \approx 10^{-11}$ N for an effective elastic coefficient and $\Delta\varepsilon \approx 12$ for the dielectric anisotropy, the corresponding electric coherence length [15], $\xi = \{K/(\varepsilon_0 \cdot \Delta\varepsilon)\}^{1/2} \cdot E^{-1}$, can be estimated to be of the order of $\xi \approx 10$ µm, i. e. much larger than the distance of a few hundred nanometers to which the evanescent wave of the microcavity modes are expected to extend. It should also be noted that the field-induced shift is not reversible, i. e. the peaks remain at the respective field-induced wavelength when the voltage is removed. The effect can only be repeated after the sample was heated above the clearing temperature and slowly cooled down back to the nematic state. From these two observations, we conclude that the effect observed is not due to an elastic deformation of the director field, but rather due to a very weak anchoring energy and thus to a change of the anchoring of the director at the surface. If so, the anchoring energy of the liquid crystal director at the GaAs surface should not exceed a value of roughly 10^{-7} J/m^2, which is about one order of magnitude smaller than the anchoring energy of 5 CB on a rubbed clean glass or a glass covered with poly(vinyl alcohol) [16].
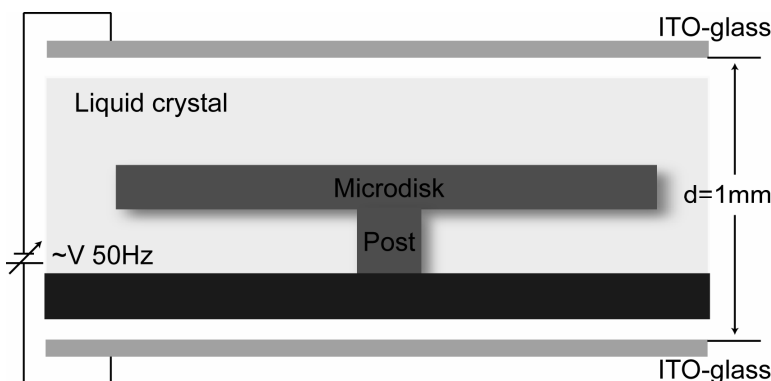

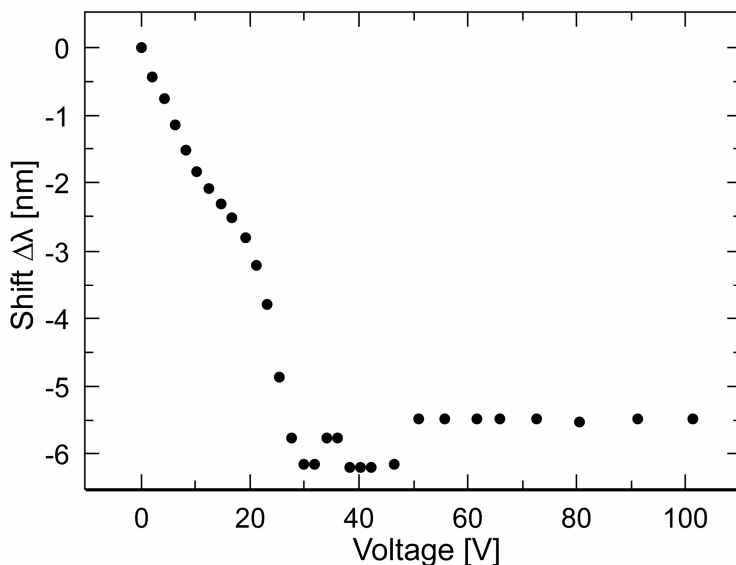**Figure 9.** Experimental setup of the sample for applying electric fields.

Figure 10. Shift of the resonance wavelengths as a function of the rms value of the applied voltage.

5. CONCLUSION

In conclusion, the large sensitivity of the dielectric constants of liquid crystals to changes of the temperature or external fields are very useful to control the optoelectronic and photonic properties of semiconductor structures. In addition to the tuning of photonic crystals (section 1), which has also been reported earlier [7-10], a novel effect is presented in this paper, namely the tuning of the emission wavelengths of microresonators based on GaAs, which are luminescent due to an active layer of InAs quantum dots. In contrast to many other optoelectronic semiconductor structures, this system works very well at ambient temperature. This is not only a benefit for possible applications but also a precondition for the effective use of liquid crystals. Fortunately, the embedding of the microdisk in the liquid crystal is not in contradiction to a high quality factor, $Q > 3500$. Spectral shifts $\Delta\lambda$ of the resonance wavelength of several nm can be induced by adjusting the temperature or by applying electric fields at moderate field strength. This shift is more than one order of magnitude larger than the spectral width ($\approx$ 0.3 - 0.4 nm) of the resonance peaks. The precise mechanism behind this useful effect still needs to be clarified. So far, it seems to be clear that changes of the effective dielectric constant in the vicinity of a microdisk have an effect on the evanescent field of the resonant eigenmodes and thus on the eigenfrequencies. Due to the preliminary results presented here, we suspect that the field-induced variations are caused by a field-induced change of the anchoring of the director rather than an elastic deformation of the director field. Further experimental studies and computer simulations are in progress to study the effects in more detail.

ACKNOWLEDGEMENTS

REFERENCES

1. H.-S. Kitzerow and J. P. Reithmaier: "Tunable Photonic Crystals using Liquid Crystals", chapter in "*Photonic Crystals: Advances in Design, Fabrication and Characterization*", edited by: K. Busch, S. Lölkes, R. B. Wehrspohn, and H. Föll, Wiley-VCH, Weinheim, 2004.
2. Tuning the optic response of photonic bandgap structures III, edited by Paul V. Braun and Sharon M. Weiss, Proc. SPIE **6322** (2006). Tuning the optical response of photonic bandgap structures II, edited by P. M. Fauchet and P. V. Braun, Proc. SPIE **5926** (2005). Tuning the optical response of photonic bandgap structures, edited by P. M. Fauchet and P. V. Braun, Proc. SPIE **5511** (2004).
3. H.-S. Kitzerow, A. Lorenz, and H. Matthias: "Tunable photonic crystals obtained by liquid crystal infiltration", Phys. Stat. Sol. (a) **204 (11)**, 3754-3767 (2007).
4. K. Busch and S. John: "*Liquid-Crystal Photonic-Band-Gap Materials: The Tunable Electromagnetic Vacuum*", Phys. Rev. Lett. **83**, 967-970 (1999).
5. K. Yoshino, Y. Shimoda, Y. Kawagishi, K. Nakayama, and M. Ozaki: "Temperature tuning of the stop band in transmission spectra of liquid-crystal infiltrated synthetic opal as tunable photonic crystal", Appl. Phys. Lett. **75**, 932-934 (1999).
6. S. W. Leonard, J. P. Mondia, H. M. van Driel, O. Toader, S. John, K. Busch, A. Birner, U. Gösele, and V. Lehmann: „Tunable two-dimensional photonic crystals using liquid crystal infiltration", Phys. Rev. B **61**, R2389-R2392 (2000).
7. G. Mertens, T. Röder, H. Matthias, H. Marsmann, H.-S. Kitzerow, S.-L. Schweizer, C. Jamois, R.-B. Wehrspohn, and M. Neubert: „Two- and three-dimensional photonic crystals made of macroporous silicon and liquid crystals", Appl. Phys. Lett. **83**, 3036-3038 (2003).
8. G. Mertens, R. B. Wehrspohn, H.-S. Kitzerow, S. Matthias, C. Jamois, and U. Gösele: „Tunable defect mode in a three-dimensional photonic crystal", Appl. Phys. Lett. **87**, 241108 (2005).

SPIE USE: ـــــ DB Check, ـــــ Prod Check, Notes:

9. H. Matthias, T. Röder, R. B. Wehrspohn, H.-S. Kitzerow, S. Matthias, and S. J. Picken: "Spatially periodic liquid crystal director field appearing in a photonic crystal template", Appl. Phys. Lett. **87**, 241105 (2005).

10. H. Matthias, S. L. Schweizer, R. B. Wehrspohn, and H.-S. Kitzerow: "Liquid Crystal Director Fields in Micropores of Photonic Crystals", Journal of Optics A, Special Issue about the 1st Nanometa Conference (Seefeld, Austria, 2007), J. Opt. A: Pure Appl. Opt. **9**, 389-395 (2007).

11. C. Schuller, F. Klopf, J. P. Reithmaier, M. Kamp, and A. Forchel: "Tunable photonic crystals fabricated in III-V semiconductor slab waveguides using infiltrated liquid crystals", Appl. Phys. Lett. **82**, 2767-2769 (2003).

12. B. Maune, M. Loncar, J. Witzens, M. Hochberg, T. Baer-Jones, D. Psaltis, A. Scherer, and Y. Qiu: "Liquid-crystal electric tuning of a photonic crystal laser", Appl. Phys. Lett. **85**, 360-362 (2004).

13. S. L. McCall, A. F. J. Levi, R. E. Slusher, S. J. Pearton, and R. A. Logan, Appl. Phys. Lett. **60**, 289 (1992).

14. W. S. Lau, E. F. Chor, S. P. Kek, W. H. bin Abdul Aziz, H. C. Lim, C. H. Heng, and R. Zhao, Jpn. J. Appl. Phys. 36, 3770-3774 (1997).

15. P. G. de Gennes and J. Prost, *The physics of liquid crystals*, 2nd edition, Clarendon Press, Oxford, 1993.

16. L. M. Blinov and V. G. Chigrinov: *Electrooptic Effects in Liquid Crystal Materials*, Springer-Verlag, New York, 1994.